Controllable trions in buckled two-dimensional materials

Roman Ya. Kezerashvili [1,2] Shalva M. Tsiklauri [3] and Anastasia Spiridonova [1]

[1]*New York City College of Technology*, The City University of New York, New York, New York 11201, USA
[2]*The Graduate School and University Center*, The City University of New York, New York, New York 10016, USA
[3]*Borough of Manhattan Community College*, The City University of New York, New York, New York 10007, USA

We predict the formation of intravalley and intervalley controllable trions in buckled two-dimensional (2D) materials such as silicene, germanene, and stanene monolayers in an external electric field. A study is performed within the framework of a nonrelativistic potential model using the method of hyperspherical harmonics (HH). We solve the three-body Schrödinger equation with the Rytova-Keldysh potential by expanding the wave functions of a trion in terms of the HH. A resultant system of coupled differential equations is solved numerically. Controllable ground-state energies of intravalley and intervalley trions by the external electric field are presented. The dependencies of the binding energy (BE) of trions in silicene, germanene, and stanene as a function of the electric field are qualitatively similar. BEs of trions formed by *A* and *B* excitons have a non-negligible difference that increases slightly as the electric field increases. It is demonstrated that trion BEs can be controlled by the external electric field, and the dielectric environment has a significant effect on the trion BE. The capability to control the BE and compactness of trions in buckled 2D materials by an external electric field suggests a possible trions crystallization in Xenes.

I. INTRODUCTION

The prediction of trions [1] consisting of an exciton and an electron or a hole, known as negatively or positively charged excitons ($X^{\mp}$), gave rise to many theoretical and experimental studies of trions in bulk materials, quantum-well systems, and two-dimensional (2D) materials. Atomically thin transition-metal dichalcogenides (TMDCs) are a class of 2D materials with remarkable optical and electronic properties [2,3]. Since 2013, when trions were observed in two-dimensional MoS_2 monolayers [4], trions have been the subject of intense studies, both experimentally and theoretically, in monolayer TMDCs. In the past decade, different experimental groups have observed and reported the signature of a trion in TMDC monolayers.

Theoretical studies of trions have integrated a wide variety of techniques and carried them out to calculate the binding energies (BEs) of excitonic complexes in monolayer TMDCs (see the reviews [5–9]). The first calculations of the BEs of trions in TMDC were performed using the variational method, and then different approaches were used in calculations such as the stochastic variational method with a correlated Gaussian basis, the diffusion quantum Monte Carlo and path-integral Monte Carlo methods, a direct diagonalization of the three-particle Hamiltonian within the Tamm-Dancoff approximation, the finite-element method, the hyperspherical harmonic method, and three-body Faddeev equations in configuration or momentum spaces, which we are citing in chronological order [10–38]. Results for BEs of trions in TMDC monolayers yielded impressively accurate results consistent with experimental data.

Another category of 2D semiconductors are the buckled 2D allotropes of silicon, germanium, and tin, known as silicene, germanene, and stanene, and collectively referred to as Xenes [39,40]. Experimental studies revealed one of the most crucial differences between Xenes and graphene and TMDC, i.e., that Xenes monolayer is not a perfectly flat sheet, but instead is slightly buckled [39,41]. As a result, this unique structure of Xenes makes them sensitive to the external electric field applied perpendicular to the monolayer, allowing the band gap to be opened and controlled. The tunable band gap of Xenes gives researchers, among other things, extraordinary *in situ* control over binding energies and optical properties of excitons in these materials.

In contrast to TMDCs, there is no extensive research on excitonic complexes in Xenes monolayers. The reason is that the synthesis of Xenes monolayers has not been as successful and extensive as, for example, TMDC monolayers because Xenes monolayers are unstable in the air [42,43]. In contrast to graphene, silicene and other Xenes monolayers do not occur in nature. Nevertheless, silicene nanoribbons were experimentally synthesized on a metal substrate [44,45]. This opened the way for silicene, germanene, and stanene monolayers to be transferred on metal such as Au [46–50] and substrates such as MoS_2, Ir, ZrB_2 [49,51], and hexagonal boron nitride (hBN) [52,53], and synthesized as freestanding monolayers [54]. Working with a metallic substrate is easier. For example, silicene grown on Ag (111) [43,55] and germanene synthesized by dry deposition on the Au (111) surface [48] have been thoroughly investigated. However, depositing Xene on a metal leads to a significant alteration of properties of the Xene monolayer. Depending on a substrate, the properties of Xenes monolayers vary; see Refs. [39,52] for the list of Xenes properties on different substrates. In contrast to deposition on a metal, depositing Xenes on hBN is harder. However, Xene deposited on hBN preserves its properties because Xene and

hBN weakly interact [52]. Xenes monolayers deposited on hBN present a particular interest for studying magnetoexcitons in monolayers and vdWHs [56].

Xenes optical and magneto-optical properties have been addressed in Refs. [41,57–59] and [60,61], respectively. Different physical phenomena, such as the Hall effect [55], the valley-locked spin-dependent Seebeck effect [62], the anomalous quantum Hall effect [47], the quantum spin Hall effect [63], and the Landau levels [55,60,64] are studied because of their essential role in applications of Xenes monolayers in nanodevices and quantum devices [63,65–68].

Because of the band inversion, these honeycomb materials are also topological insulators [69–74]. The existence of an excitonic insulator phase in silicene, germanene, and stanene was first studied by Brunetti et al. [75,76] in the framework of the effective-mass approximation. The influence of the screening, band dispersion, and external electric field on transitions in Xenes between excitonic, topological, and trivial insulator phases was investigated in [77].

A summary of the available Xenes, including their intrinsic properties and schemes for synthesis, along with an overview of the technological and scientific framework where Xenes may bring promising advances, is given in Ref. [78], which was published exactly 10 years after the discovery of silicene.

Currently, there is a shortage of research on exciton complexes in Xenes. In particular, there has not been a study of the formation of three quasiparticle states—trions—in Xenes monolayers. In this paper, we address this gap and focus on a theoretical investigation of trions in Xenes within the method of hyperspherical harmonics (HH).

The paper is organized as follows. In Sec. II, we present the theoretical model and formalism to study Mott-Wannier trions in Xenes within the framework of the method of hyperspherical harmonics. We consider a nonrelativistic potential model for a system of three interacting electrons and holes, and we employ the three-body Schrödinger equation in the effective-mass approximation. In the framework of the HH method, the Schrödinger equation with the Rytova-Keldysh potential [79,80] is reduced to a system of coupled differential equations for hyperradial functions. A numerical solution of this system provides the BE and wave function for trions in Xenes. In Sec. III, we discuss a classification of intravalley and intervalley trions in Xenes monolayers (Sec. III A), and we present results of calculations of controllable ground-state energies of intravalley and intervalley trions by an external electric field (Sec. III B). Here we analyze the dependencies of the BEs and probability distributions of three bound particles on the external electric field. Based on the capability to control a BE and the compactness of trions in Xenes by the external electric field, we discuss a proposal of a possible trions crystallization in Xenes, and we estimate corresponding densities of composite fermions gas. Conclusions follow in Sec. IV.

II. THEORETICAL MODEL

We start by providing the framework of the low-energy model describing exciton states in Xenes monolayers and heterostructures when the external electric field perpendicular to a monolayer is present. Silicene, germanene, and stanene monolayers are 2D buckled materials and have honeycomb-

structure-like graphene. However, in contrast to graphene, the most stable form of Si, Ge, and Sn monolayers is the honeycomb lattice with the offset of triangular sublattices A and B with respect to the monolayer's plane. The offset is denoted by d_0 and is known as the buckling constant or buckling factor. As a result of the buckled structure of Xenes monolayers, they are sensitive to the external electric field applied perpendicular to a monolayer. This manifests as an on-site potential difference between sublattices when the electric field is applied. When the external electric field is not applied, the band structure of Xenes monolayers in the vicinity of the K/K' points resembles a graphene band structure. However, the intrinsic gaps of Xenes are larger than the band gaps in graphene. The application of the external electric field perpendicular to the monolayer leads to a potential difference between sublattices A and B that changes the band gap, resulting in changes in the effective masses of the electrons and holes.

The single-particle Hamiltonian of electronic states in monolayer Xenes in the electric field acting along the z-axis in the vicinity of the K/K' points reads ($\hbar = c = 1$) [81]

$$\hat{H} = v_F(\xi p_x \hat{\tau}_x + p_y \hat{\tau}_y) - \xi \Delta_{\text{gap}} \hat{\sigma}_z \hat{\tau}_z + \Delta_z \hat{\tau}_z. \quad (1)$$

In Eq. (1), v_F is the Fermi velocity, $\xi, \sigma = \pm 1$ are the valley and spin indices, respectively, p_x and p_y are the components of momentum in the xy-plane of the monolayer relative to the K point, $\hat{\tau}$ and $\hat{\sigma}$ are the pseudospin and real spin Pauli matrices, respectively, $2\Delta_{\text{gap}}$ is the intrinsic band gap, and $\Delta_z = ed_0 E_\perp$ is the gap induced by the electric field, $E_\perp$, acting along the z-axis. The first term in Hamiltonian (1) is the same as that of the low-energy Hamiltonian in graphene [82,83], the second term is the spin-orbit coupling with an intrinsic band gap of $2\Delta_{\text{gap}}$, and the last term describes the sublattice potential difference appearing when the external electric field is applied [46,47,84,85].

From Eq. (1), the low-energy eigenvalues for charge carriers near the K/K' points can be written as [81]

$$E(k) = \sqrt{\Delta_{\xi\sigma}^2 + v_F^2 p^2}, \quad (2)$$

where

$$\Delta_{\xi\sigma} = |\xi\sigma \Delta_{\text{gap}} - ed_0 E_\perp| \quad (3)$$

is the electric-field-dependent band gap at $p = 0$. When there is no external electric field, the spin-up and spin-down bands of the valence and conduction bands are degenerate. Application of $E_\perp$ lifts this degeneracy by splitting both the valence and conduction bands. When $\xi = -\sigma$, the gap is large, since conduction and valence bands are the furthest from the Fermi energy level, and the electron and hole form A excitons. When $\xi = \sigma$, the gap is small, since conduction and valence bands are the closest, and the electron and hole form B excitons. To open the band gap $\Delta_{\xi\sigma}$, a critical value of the electric field has to be achieved, $E_c = \Delta_{\text{gap}}/(ed_0)$, and then the lower bands form a Dirac cone at the K/K' points. The critical values of the electric field for Xenes monolayers are given in Ref. [76]. Parabolic conduction and valence bands in the vicinity of the K/K' points allow us to find the effective mass of charge carriers as $m = \Delta_{\xi\sigma}/v_F^2$. In Xenes monolayers the lowest conduction and the highest valence bands are symmetric, therefore the effective masses of an electron and hole

are the same and can be written as a function of the external electric field:

$$m = \frac{|\xi \sigma \Delta_{\text{gap}} - ed_0 E_\perp|}{v_F^2}. \tag{4}$$

Analysis of Eq. (4) shows that the value of the electron or hole effective mass depends on the band gap, Fermi velocity, and buckling constant, and it is a function of $E_\perp$.

A. Effective-mass approach for trions in buckled 2D materials

The promotion of an electron from the filled valence band to the empty conduction band leaves an empty electron state in the valence band. The description of such a many-body system can be reduced to the two-particle problem of a negatively charged conduction electron interacting with a positively charged valence hole that forms an exciton or other excitonic complexes such as charged excitons or trions. The trions are formed when an exciton binds another electron or hole to form a negatively or positively charged three-particle system: X^- or X^+, respectively. A description of the properties of trions requires a solution of a three-particle problem. In buckled two-dimensional monolayers, the resulting trions are considered as Wannier-Mott trions since the correlation between an electron and a hole extends over many lattice periods. The representation of the electron-hole pair bound in a Wannier-Mott exciton shows the strong spatial correlation of these two constituents. Therefore, we are assuming that the interaction of the exciton with the third particle (electron or hole) leads to a large-radius-type system.

We follow the approach in which one assumes that the electron and hole bands are isotropic and parabolic, which is a good approximation for the low-energy spectrum of 2D materials. This form of the Hamiltonian implies that both the electron and hole single-particle states form a single parabolic band. The corresponding eigenproblem equation reduces to the Schrödinger equation in the effective-mass approximation. This approach is commonly used in the literature to describe excitons and trions in 2D materials. See, for example, Refs. [2,3,6,8,10,38,86–88]. Below, we follow the effective-mass approximation.

To obtain the eigenfunctions and eigenenergies of a 2D trion in Xenes when the electric field is perpendicular to the Xenes monolayer, we write the Schrödinger equation for an interacting three-particle electron-hole system. Because we are considering the varying electric field $E_\perp$, which is directed along the z-axis, the corresponding term in the 2D Schrödinger equation vanishes. However, the effect of the electric field action is present through the effective mass as follows from Eq. (4). Thus, one can write the 2D Schrödinger equation for the interacting three-particle electron-hole system within the effective-mass approximation in the following form:

$$\left[-\frac{\hbar^2}{2} \sum_{i=1}^{3} \frac{1}{m_i} \nabla_i^2 + \sum_{i<j}^{3} V_{ij}(|\mathbf{r}_i - \mathbf{r}_j|) \right] \Psi(\mathbf{r}_1, \mathbf{r}_2, \mathbf{r}_3)$$
$$= E \Psi(\mathbf{r}_1, \mathbf{r}_2, \mathbf{r}_3), \tag{5}$$

where m_i is the effective mass of the electron or hole defined by Eq. (4), and $\mathbf{r}_i$ is the ith particle position. We assume

only two types of charge carriers: an electron and hole with the corresponding effective masses. In Eq. (5), $V_{ij}(|\mathbf{r}_i - \mathbf{r}_j|)$ is the interaction potential between q_i and q_j charges in a 2D material that was first derived in Ref. [79] and was independently obtained by Keldysh [80]. We refer to it as the Rytova-Keldysh (RK) potential. The RK potential describes the Coulomb interaction screened by the polarization of the electron orbitals in the 2D lattice and has the following form:

$$V_{ij}(r) = \frac{\pi k q_i q_j}{2\kappa \rho_0} \left[H_0\left(\frac{r}{\rho_0}\right) - Y_0\left(\frac{r}{\rho_0}\right) \right], \tag{6}$$

where $r = |\mathbf{r}_i - \mathbf{r}_j|$ is the relative coordinate between two charge carriers q_i and q_j. In Eq. (6), $k = 9 \times 10^9 \, \text{N m}^2/\text{C}^2$, κ is the dielectric constant of the environment that is defined as $\kappa = (\varepsilon_1 + \varepsilon_2)/2$, where ε_1 and ε_2 are the dielectric constants of two materials that surround the Xenes layer, ρ_0 is the screening length, which sets the boundary between two different behaviors of the potential due to a nonlocal macroscopic screening, and $H_0(\frac{r}{\rho_0})$ and $Y_0(\frac{r}{\rho_0})$ are the Struve function and Bessel function of the second kind, respectively. The screening length ρ_0 can be written as $\rho_0 = (2\pi \chi_{2D})/(\kappa)$ [10], where χ_{2D} is the 2D polarizability, which in turn is given by $\chi_{2D} = l\varepsilon/4\pi$ [80], where ε is the bulk dielectric constant of the Xene monolayer. For large distances $r \gg \rho_0$, the potential has the three-dimensional bare Coulomb tail $V_{ij}(r) = \frac{kq_i q_j}{\epsilon r}$, while at very small distances, smaller than the screening length $r \ll \rho_0$, it becomes a logarithmic potential like a potential of a point charge in two dimensions: $V_{ij}(r) = \frac{kq_i q_j}{\epsilon \rho_0}[\ln(\frac{r}{2\rho_0}) + \gamma]$, where γ is the Euler constant. Therefore, the potential (6) becomes the standard bare Coulomb potential at $r \gg \rho_0$ and diverges logarithmically at $r \ll \rho_0$. A crossover between these two regimes takes place around distance ρ_0. Thus, at small distances between charge carriers, the short-range interaction strength decreases, while the long-range interaction strength is unaffected and is the bare three-dimensional Coulomb potential. It is worth noting that in Ref. [89], a very good approximation to the RK potential that is simpler to use, fairly precise in both limits, and remarkably accurate for all distances was introduced.

To obtain a solution of the Schrödinger equation (5) for the negatively and positively charged trions, we use the method of hyperspherical harmonics (HH) [90]. The main idea of this method is the expansion of the wave function of the trion in terms of HH, which are the eigenfunctions of the angular part of the Laplace operator in the four-dimensional (4D) space. As the first step, let us separate the center-of-mass (c.m.) and the relative motion of three particles and introduce sets of mass-scaled Jacobi coordinates [90,91]. There are three equivalent sets of Jacobi coordinates, and there is an orthogonal transformation between these sets [92,93]. For three nonidentical particles that have different masses, the mass-scaled Jacobi coordinates for the partition i read as follows [90–92]:

$$\mathbf{x}_i = \sqrt{\frac{m_j m_k}{(m_j + m_k)\mu}} (\mathbf{r}_j - \mathbf{r}_k),$$

$$\mathbf{y}_i = \sqrt{\frac{m_i(m_j + m_k)}{(m_i + m_j + m_k)\mu}} \left(\frac{m_j \mathbf{r}_j + m_k \mathbf{r}_k}{m_j + m_k} - \mathbf{r}_i \right),$$

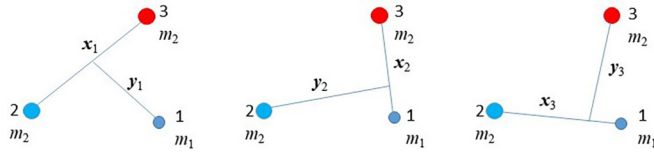$$i \neq j \neq k = 1, 2, 3, \tag{7}$$

FIG. 1. Schematics of partition trees of Jacobi coordinates when two particles have the same masses. The electron and hole in one electron-hole pair have the same masses. This corresponds to the intravalley X^- and X^+ trions.

where

$$\mu = \sqrt{\frac{m_i m_j m_k}{m_i + m_j + m_k}} \qquad (8)$$

is the three-particle effective mass. In Eqs. (7), the subscripts i, j, and k are a cyclic permutation of the particle numbers. Trees of Jacobi coordinates for a three-particle system, when two particles have the same masses, are shown in Fig. 1.

The transformation (7) allows the separation of c.m. and relative motions of three particles with Hamiltonian (5), and the Schrödinger equation for the relative motion of the three-body system reads

$$\left[-\frac{\hbar^2}{2\mu} \left(\nabla_{x_i}^2 + \nabla_{y_i}^2 \right) + V(x_1) + V(x_2) + V(x_3) \right] \Psi(\mathbf{x}_i, \mathbf{y}_i)$$
$$= E \Psi(\mathbf{x}_i, \mathbf{y}_i). \qquad (9)$$

In Eq. (9), $V(x_i)$ is the interaction potential between two particles at the relative distance x_1, x_2, and x_3, respectively, where x_i is the modulus of the Jacobi vector $\mathbf{x}_i$ (7), and (9) is written for any of the set $i = 1, 2, 3$ of the Jacobi coordinates (7). The orthogonal transformation between three equivalent sets of the Jacobi coordinates simplifies calculations of matrix elements involving $V(x_i)$ potentials.

This method is presented in detail in Ref. [38] and is briefly outlined here. We introduce in the 4D space the hyperradius $\rho = \sqrt{x_i^2 + y_i^2}$ and a set of three angles $\Omega_i \equiv (\alpha_i, \varphi_{x_i}, \varphi_{y_i})$, where φ_{x_i} and φ_{y_i} are the polar angles for the Jacobi vectors $\mathbf{x}_i$ and $\mathbf{y}_j$, respectively, and α_i is an angle defined as $x_i = \rho \cos \alpha_i$, $y_i = \rho \sin \alpha_i$. Next, we rewrite the Schrödinger equation (9) for the trion using hyperspherical coordinates in the 4D configuration space [38]. This transformation allows us to reduce the solution of the problem for the three particles in the 2D configuration space to the motion of one particle in the 4D configuration space. Then we introduce the hyperspherical harmonics $\Phi_{K\lambda}(\Omega)$ in the 4D configuration space, which are the eigenfunctions of the angular part of the generalized Laplace operator $\widehat{K}^2(\Omega_i)$ in the 4D configuration space $\widehat{K}^2(\Omega_i)\Phi_{K\lambda}(\Omega) = K(K+2)\Phi_{K\lambda}(\Omega)$ [90], where K is a grand angular momentum. Here we are using the shorthand notation $\lambda \equiv \{l_x, l_y, L, M\}$, where L is the total orbital angular momentum of the trion, M is its projection, and the grand angular momentum $K = 2n + l_x + l_y$, where l_x and l_y are the angular momentum corresponding to $\mathbf{x}$ and $\mathbf{y}$ Jacobi coordinates, respectively, and $n \geqslant 0$ is an integer number.

The functions $\Phi_{K\lambda}(\Omega)$ present a complete set of orthonormal basis, and we can expand the wave function of the trion
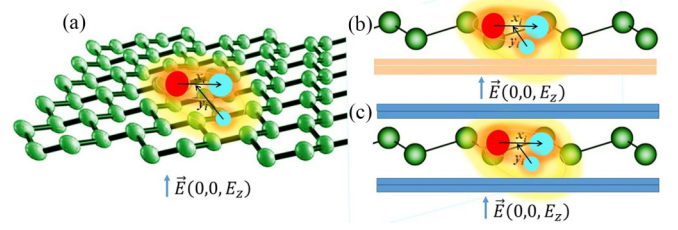

FIG. 2. Schematic representation of the X^- trion in the external electric field perpendicular to the Xene layer in (a) freestanding, (b) supported, and (c) encapsulated Xenes monolayer. x_i and y_i are Jacobi coordinates for the partition i.

$\Psi(\rho, \Omega_i)$ in terms of the HH $\Phi_{K\lambda}(\Omega)$ as

$$\Psi(\rho, \Omega_i) = \rho^{-3/2} \sum_{K\lambda} u_{K\lambda}(\rho) \Phi_{K\lambda}(\Omega_i). \qquad (10)$$

In Eq. (10), $u_{K\lambda}(\rho)$ are the hyperradial functions, and by substituting (10) into the Schrödinger equation written in the hyperspherical coordinates [38], one can separate the radial and angular variables and get a set of coupled differential equations for the hyperradial functions $u_{K\lambda}(\rho)$:

$$\left[\frac{d^2}{d\rho^2} - \frac{(K+1)^2 - 1/4}{\rho^2} + \kappa^2 \right] u_{K\lambda}(\rho)$$
$$= \frac{2\mu}{\hbar^2} \sum_{K'\lambda'} \mathcal{W}_{K\lambda K'\lambda'}(\rho) u_{K'\lambda'}(\rho). \qquad (11)$$

In Eq. (11), $\kappa^2 = 2mB/\hbar^2$, where B is the trion BE. The coupling effective potential energy $\mathcal{W}_{K\lambda K'\lambda'}(\rho)$ is

$$\mathcal{W}_{K\lambda K'\lambda'}(\rho) = \int \Phi_{K\lambda}^*(\Omega_i) \sum_{i<j}^{3} V_{ij}(|\mathbf{r}_i - \mathbf{r}_j|) \Phi_{K'\lambda'}(\Omega_i) d\Omega_i. \qquad (12)$$

The coupling effective interaction (12) is defined via the RK potential (6). Substituting Eq. (6) into Eq. (12), one obtains the matrix elements of the effective potential energies. The method of calculations of the effective potential energies is given in [38]. Calculations of matrix elements $\mathcal{W}_{K\lambda K'\lambda'}(\rho)$ of the two-body $V_{ij}(|\mathbf{r}_i - \mathbf{r}_j|)$ interactions in the hyperspherical harmonics expansion method for a three-body system are greatly simplified by using the HH basis states appropriate for the partition corresponding to the interacting pair. Using the matrix elements $\mathcal{W}_{K\lambda K'\lambda'}(\rho)$ in Eq. (11), one can solve the system of coupled differential equations numerically. Results of numerical solutions of (12) for trions in Xenes are presented in the next section.

III. TRIONS IN XENES

We apply the present theoretical approach for calculations of the trion BEs in the following Xenes monolayers: silicene (Si), germanene (Ge), and stanene (Sn). A schematic representation of a trion in freestanding, supported, and encapsulated Xenes monolayers in the external electric field $E_z = E_\perp$ perpendicular to the Xene layer is given in Fig. 2. The formation of the trion wave function (10) is the most general, not restricted to any particular mass ratio of electrons and holes,
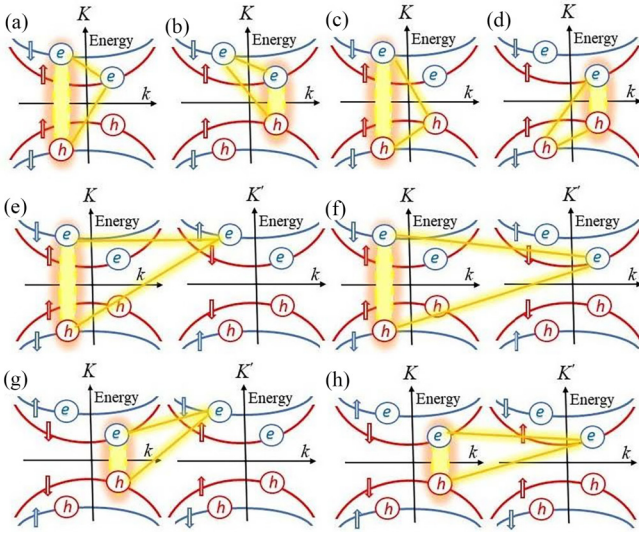
FIG. 3. Schematic representation of the low-energy band structure for 2D Xenes material and formation of the intravalley X^- and X^+ trions and intervalley X^- trions. Panels (a),(b) and (c),(d) represent the intravalley X^- and X^+, respectively. Panels (e), (f), (g), and (h) correspond to the intervalley X^- trions with the decreasing masses from the biggest [spin-valley configuration (e)] to the smallest [spin-valley configuration (h)]. Intervalley X^+ trions have the same masses as X^-.

and describes the three-particle relative motion. The splitting of the conduction and valence bands in Xenes due to spin-orbit coupling at nonzero electric fields leads to the formation of A and B excitons in the larger or smaller band gaps, with corresponding larger or smaller masses of the electron and hole. Two of the three particles constituting a positive or a negative trion in the Xene monolayer have the same masses due to the equity of the mass of the electron and hole that form an exciton. However, they are not identical because they have different charges. An intervalley trion may have the same masses of three particles, but they are not identical due to the different spin and/or valley indices. Below we consider trions formed by a singlet bright A or B exciton and an electron (X^-) or hole (X^+). The trion can be in either a single or a triplet state.

A. Intravalley and intervalley trions

In a 2D monolayer of Xenes, intravalley and intervalley trions can be formed. Let us first consider intravalley trions. An interaction of a bright A or B exciton with another charged carrier in the same valley, which can either be an electron or a hole, forms an X^- or X^+ intravalley trion. The schematics in Fig. 3 show the possible formations of X^- [Figs. 3(a) and 3(b)] and X^+ [Figs. 3(c) and 3(d)]. As follows from Eq. (4), the electron and hole effective masses in the A exciton are the same. The B excitons are composed of an electron and hole that also have equal masses but smaller masses than those of the electron and hole in A excitons. We denoted these masses as m_A and m_B, respectively. The intravalley X^- and X^+ trions have the same two particles masses. As follows from Eq. (8), the effective masses of the X^- and X^+ trions formed by an A or B exciton are $\mu_A = \sqrt{\frac{m_B m_A^2}{m_B + 2m_A}}$ and $\mu_B = \sqrt{\frac{m_A m_B^2}{m_A + 2m_B}}$,

respectively [38]. Because $m_A > m_B$, it follows that $\mu_A > \mu_B$. Therefore, the effective mass of the X^- and X^+ trions formed by the A exciton is larger than the mass of the X^- and X^+ trions formed by the B exciton. Due to the proportionality of the BE of trions to the three-particle effective mass μ [38], a BE of X^- and X^+ trions formed by the A exciton is larger than the BE of trions formed by the B exciton. In the ground state, both intravalley trions formed by charge carriers from the same valley are spin-singlet trions.

Intervalley X^- trions result from the attraction between K valley bright A excitons with an electron from the K' valley or bright B excitons from the K valley with an electron from the K' valley. The effective masses of the X^- intervalley trions formed by bright A excitons are always larger than the effective masses of trions formed by B excitons. The corresponding spin-valley configurations are presented in Figs. 3(e)–3(h). We should mention that the intervalley X^+ trions have the same masses as the X^- trions formed by the K valley bright A and B excitons due to the interaction with a hole from the K' valley. While intravalley trions are composed of two particle with the same masses, intervalley trions can be a system of three particles with the same masses [Figs. 3(e) and 3(h)] or a three-particle system with two particles that have the same masses [Figs. 3(f) and 3(g)].

B. Results of calculations

The intravalley X^- and X^+ trions in Xenes monolayers have two particles (the electron and hole) that have the same masses, and the third particle (the electron or hole) has a different mass, as seen in Figs. 3(a)–3(d). Therefore, we have to deal with three nonidentical particles because two particles with the same masses have different charges. For intervalley trions we have two cases: X^- and X^+ trions formed by the electron and hole with the same masses, and the third particle has a different mass [spin-valley configurations in Figs. 3(f) and 3(g)] or all three particles have the same masses [spin-valley configurations in Figs. 3(e) and 3(h)]. In the latter case, while three particles have the same masses, two belong to different valleys.

In calculations of the BEs of trions in Xenes monolayers, we use the RK potential. We solve the system of coupled differential equations (11) for the hyperradial functions $u_{K\lambda}^L(\rho)$ numerically. By solving the system of equations (11), one finds the binding energy as well as the corresponding hyperradial functions. The latter allows one to construct the wave function (10). Numerical solution of the coupled differential equations requires the control of the convergence of the BEs for trions with respect to the grand angular momentum K for each value of the external electric field. The relative convergence of the BE is checked as $\Delta B/B = [B(K+2) - B(K)]/B(K)$, where $B(K)$ is the BE for the given K. The analysis of the results for the BEs at different values of the electric field shows that reasonable convergence is reached for $K_{\max} = 14$, so we limit our considerations to this value. The convergence of the BE depends on the trion total mass, i.e., the applied external electric field. In Fig. 4 we show the convergence of BEs obtained with RK potential as a function of K for the intervalley X^- for configurations (e) and (h), which correspond to the maximum and minimum
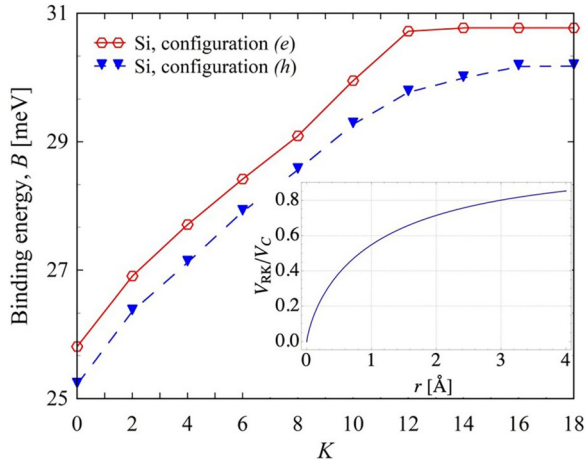
FIG. 4. Convergence for the binding energy for the intervalley X^- for configurations (*e*) and (*h*) with the maximum and minimum trion mass, respectively. Inset: The ratio of the Rytova-Keldysh to Coulomb potentials for electron-hole interaction in Si monolayer as a function of the electron-hole separation.

trion mass, respectively. The results for the convergence for other configurations are between these two limited cases. Although the results converged quite well for the RK potential, calculations with the Coulomb potential require consideration of a more grand angular momentum K for each value of the external electric field because the Coulomb potential is much stronger than the RK potential. The inset in Fig. 4 demonstrates this fact.

We considered the formation of trions in the singlet and triplet ground states, and we computed the corresponding BEs. The input parameters for calculations of BEs of trions in the freestanding, supported on SiO_2, and encapsulated by hBN Xene monolayers are presented in Table I. The formation of Wannier-Mott excitons due to the electron-hole interaction via the RK potential in semiconducting phases in Xenes monolayers occurs when the external electric field exceeds some critical value that is unique to each material [75]. A value of the critical electric field is slightly different for *A* excitons and for *B* excitons. Following *ab initio* calculations [46], which determined that the crystal structure of silicene becomes unstable around 2.6 V/Å, we consider in our calculations electric fields up to 2.7 V/Å, and we study the formation of trions in Xenes at the range of the external electric field from the critical value up to 2.7 V/Å. Results of calculations

of dependencies of trion BEs on the external electric field are presented in Fig. 5.

The results of our calculations for the BEs of intravalley trions in a singlet state in a freestanding Xenes monolayer are presented in Fig. 5(a). The BE increases for all materials as $E_\perp$ increases. In addition, in FS Si, Ge, and Sn, we observe a non-negligible difference in the BE of trions formed by *A* and *B* excitons. These differences increase slightly as the electric field increases. The trion BEs for FS Ge and FS Sn are qualitatively similar to FS Si, but they are smaller than for freestanding silicene. The curves for FS Ge and Sn qualitatively resemble that of FS silicene, but at 2.7 V/Å FS germanene reaches a maximum trions BE of 24.8 (24.3) meV, and the maximum BE for FS stanene is roughly 21.1 (20.5) meV, significantly smaller than that for FS silicene, −30.1 (29.8) meV. In parentheses, the BEs of trions formed by *B* excitons are given. The percentage differences between the trion BE of FS Si and FS Ge and that of FS Si and FS Sn at the largest electric field considered are 82% (81%) and 70% (69%), respectively.

In Fig. 5(b), the dependencies of the binding energies for intervalley singlet state trions in spin-valley configurations shown in Figs. 5(e) and 3(h) as functions of external electric field are displayed. The corresponding BEs are about 2–4% larger and qualitatively resemble that of the intravalley trions: (i) the increase of the BE as the external electric field increases; (ii) BEs for FS silicene, germanene, and stanene are qualitatively similar; (iii) a non-negligible difference in the BE of trions formed by *A* and *B* excitons.

The intravalley X^- and X^+ trions must exist in the spin-singlet state, whereas the intervalley trions can exist in either the singlet or triplet states. In Fig. 5(b) the dependencies of the binding energies for intervalley $L = 1$ and $S = 3/2$ state trions as functions of the applied external electric field are shown. The BEs of triplet state trions in the FS silicene and germanene monolayers are about three times smaller than that for singlet state trions. Our calculations show unbound triplet state trions in the FS stanene. The decrease of the trion binding energy in the triplet state is due to centrifugal repulsion.

In Fig. 5(d), the intravalley trion BEs in a Xenes monolayer supported on SiO_2 and encapsulated by hBN are presented. In our calculations, the role of the substrate and the encapsulation by hBN is considered through the potential (6) with $\kappa = (\varepsilon_1 + \varepsilon_2)/2$, where ε_1 and ε_2 are the dielectric constants of two materials that surround the Xene layer. The comparison of the BEs shows that the FS monolayers exhibit by far the largest BEs due to the much weaker dielectric screening induced by the environment compared to Xenes supported on SiO_2 or encapsulated by hBN. Hence, the trion BE is

TABLE I. Input parameters for calculations of BEs of trions in the freestanding (FS) and encapsulating Xene monolayers. The notations are the following: $2\Delta_{gap}$ is the total gap between conduction and valence bands; d_0 is the buckling parameter; v_F is the Fermi velocity; l is the monolayer thickness; ε is the dielectric constant of the Xenes monolayer; ρ_0 is the screening distance; E_c is a critical electric field.

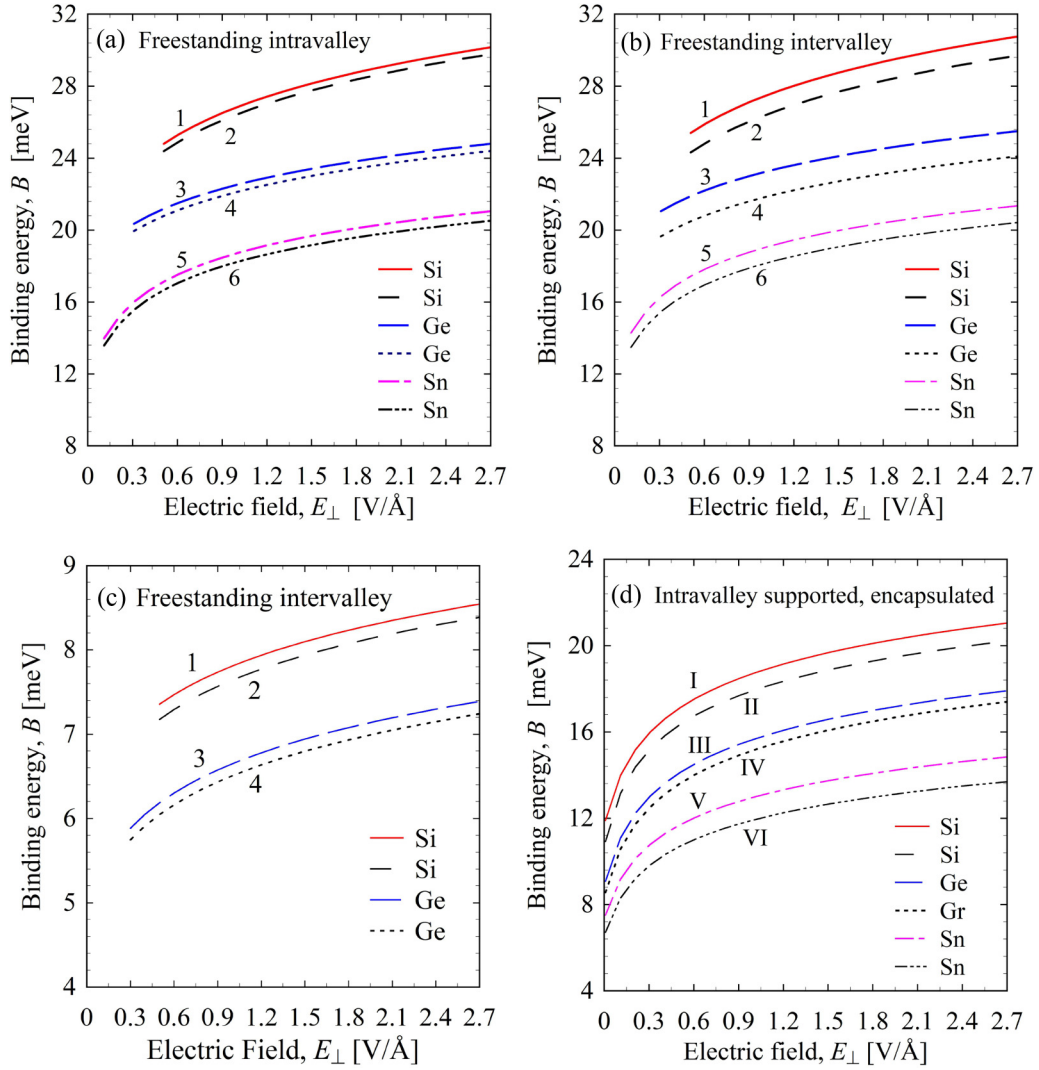| 2D material	κ	$2\Delta_{gap}$ (meV)	d_0 (Å)	$v_F \times 10^5$ (m/s)	l (nm)	ε	ρ_0 (nm)	E_c (V/Å)
FS Si	1	1.9 [94]	0.46 [95]	6.5 [94]	0.4 [43]	11.9	2.38	0.55
FS Ge	1	33 [94]	0.676 [95]	6.2 [94]	0.45	16	4.23	0.3
FS Sn	1	101 [94]	0.85 [94]	5.5 [94]	0.5	24	5.99	0.2
Si (hBN, type I)	4.89	27 [52]	0.46 [52]	4.33 [52]	0.333 [52]	11.9	0.41	None

FIG. 5. Dependencies of the BE of intravalley and intervalley trions in silicene, germanene, and stanene on the applied electric field. Curves 1, 3, and 5 correspond to the trions formed by A excitons coupling an electron (X^-) or hole (X^+), while curves 2, 4, and 6 correspond to the trions formed by B excitons coupling an electron (X^-) or hole (X^+). (a) Freestanding intravalley singlet state trions. (b) Freestanding intervalley singlet state trions. (c) Freestanding intervalley triplet state trions. (d) Intravalley singlet state trions in Xenes monolayer supported on an SiO_2 substrate (curve I, III, and V) and encapsulated by hBN (curves II, IV, and VI). The plots for FS Xenes are truncated for the external electric field $E_\perp$ less than a critical field.

the largest for the freestanding Xenes and gets progressively smaller for Xene supported on SiO_2, and it is the smallest for encapsulated by hBN. Thus, the trion BE is extremely sensitive to the dielectric environment.

We calculated a probability distribution for three particles that form a trion in the Xene. In Fig. 6, interparticle radial probability distributions for intravalley and intervalley trions in the silicene monolayer are shown. The difference in the probability distribution is related to the difference of the effective masses μ of intravalley and intervalley trions. The probability distribution for the intravalley trion is computed for the spin-valley configuration shown in Fig. 3(a), and that for the intervalley trions is calculated for the spin-valley configuration in Fig. 3(e) with the highest mass. The analysis of the dependence of the probability distributions of three particles on the hyperradius ρ and the external electric field leads to the following conclusion: the increase of the external

electric field brings an increase of the trion BE and makes trions more compact since the greater binding energy increases the probability of trion formation.

The capability to control the BE and compactness of trions in Xenes by an external electric field suggests the possibility of trion crystallization. It is well known that the dilute system of electrons can form a 2D Wigner crystal [96]. Based on the existence of trions in Xenes, we propose that trions form a 2D Wigner crystal (WC) at low densities, similar to the 2D WC formed by a dilute system of electrons.

Wigner crystallization, which was predicted 80 years ago [97], is an exotic phenomenon that represents one of the most intriguing quantum phase transitions. The first realizations of WCs [98–100] used strong magnetic fields and quasi-2D quantum-well systems. Recently, different experimental groups observed signatures of a Wigner crystallization formed in MoSe$_2$ monolayers encapsulated by hBN [101–103] and
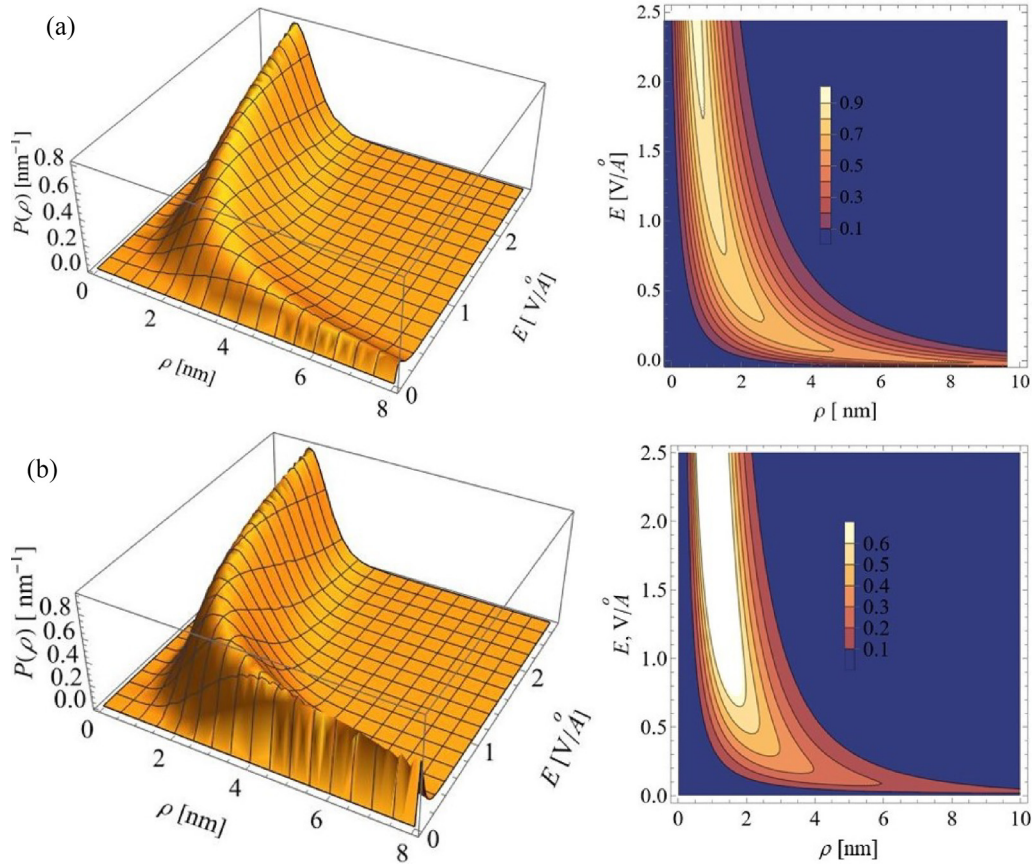
FIG. 6. Dependence of the probability distribution of three particles in freestanding silicene on hyperradius ρ and applied electric field for (a) intravalley and (b) intervalley X^- trion.

TMDC heterostructures [104–106]. An experimental study of electron crystallization in one-dimensional nanotubes [107] succeeded in imaging an electronic WC. In the past three decades, many theoretical studies were focused on 2D and 1D electron gases [108–120]. The WC formed by trions in coupled quantum wells was discussed and predicted in [121,122], while Refs. [123,124] investigated WCs at zero magnetic field and magnetic-field-induced Wigner crystallization of trions in TMDC heterostructures.

The dilute system of trions, when the average distance between them is much larger than the radius of each trion, can be treated as a dilute system of fermions with effective pair electrostatic repulsion resulting from charge-carrier interactions via the RK potential (6). It is well-established that the triangular crystal has a considerably lower energy than competing lattices in the density range of interest. Thus, to minimize the potential energy, the trions experiencing effective electrostatic repulsion undergo a phase transition and crystallize by forming a Wigner lattice. In other words, this is an example in which the WC phase occurs in a nonelectronic system at low density.

The exact interaction potential between two trions includes nine terms: five repulsive and four attractive interactions between electrons and holes. In a dilute system of trions, we can approximate the interaction between two neighboring trions separated by a distance R as three interactions: a repulsive charge-charge (electron-electron for X^- or hole-hole for X^+), an attractive interaction of a charge carrier (electron for X^-

or hole for X^+) from one trion with the exciton from the neighboring trion, and a repulsive interaction of two excitons from two neighboring trions. In other words, we treat each trion as a cluster of an exciton and a charge carrier. Therefore, the effective trion-trion interaction in the diluted system of trions can be treated as the charge-charge, charge-dipole, and dipole-dipole interactions in the 2D configuration space.

In 2D monolayers, the electrostatic charge-charge interaction is described by the RK potential (6). At large distances R between trions, the electron-electron (hole-hole) potential has a three-dimensional bare Coulomb tail $1/R$. The explicit analytical expressions for the charge-dipole and dipole-dipole interactions in 2D configuration space derived based on the potential (6) read [125]

$$V_{cd}(\mathbf{R}) = \frac{\pi k e}{2\kappa \rho_0}\left[H_{-1}\left(\frac{R}{\rho_0}\right) - Y_{-1}\left(\frac{R}{\rho_0}\right)\right]\frac{\mathbf{R}\cdot\mathbf{d}}{\rho_0 R}, \quad (13)$$

$$V_{dd}(R) = -\frac{\pi k}{2\kappa \rho_0}\left\{\left[H_{-1}\left(\frac{R}{\rho_0}\right) - Y_{-1}\left(\frac{R}{\rho_0}\right)\right]\frac{\mathbf{d_1}\cdot\mathbf{d_2}}{\rho_0 R}\right.$$
$$\left. + \left[H_{-2}\left(\frac{R}{\rho_0}\right) - Y_{-2}\left(\frac{R}{\rho_0}\right)\right]\frac{\mathbf{R}\cdot\mathbf{d_1}\mathbf{R}\cdot\mathbf{d_2}}{\rho_0^2 R^2}\right\}, \quad (14)$$

where $\mathbf{d}$ is a dipole momentum, $\mathbf{R}$ is a radius vector between a charge carrier and a dipole or between two dipoles, and $H_{-n}\left(\frac{R}{\rho_0}\right)$ and $Y_{-n}\left(\frac{R}{\rho_0}\right)$ are the Struve function and Bessel function of the second kind, respectively. Following [125], one can write the asymptotic form of (13) and (14): $V_{cd}(\mathbf{R}) \xrightarrow[R\to\infty]{}$
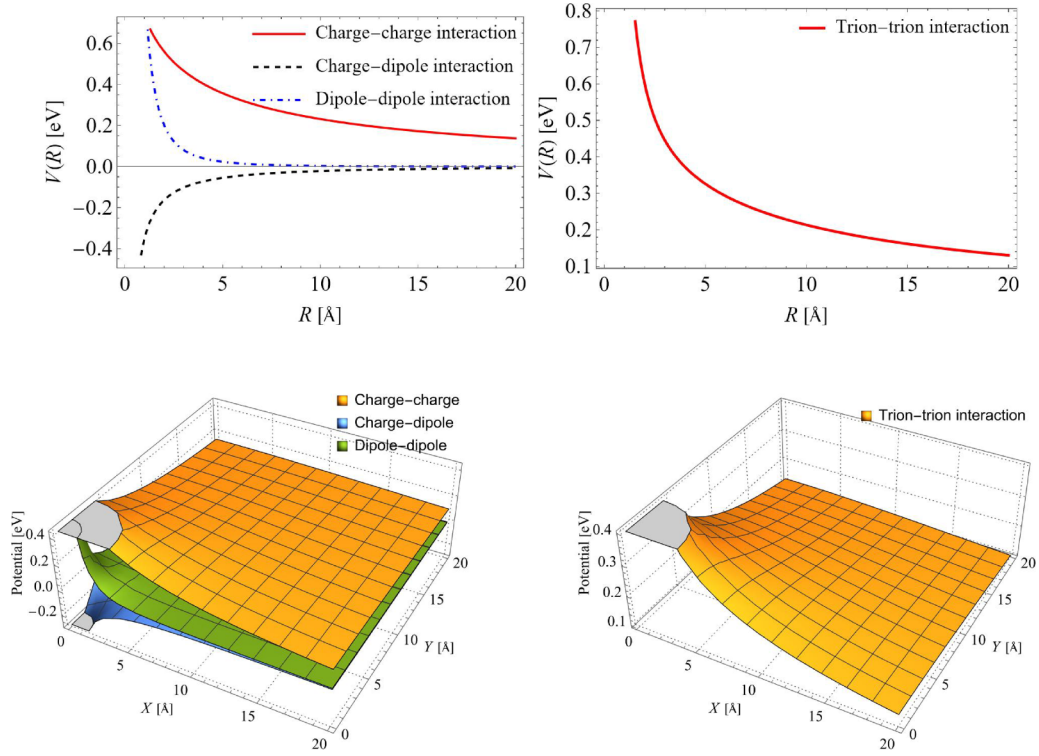
FIG. 7. The charge-charge, charge-dipole, and dipole-dipole interactions between constituent particles of two neighboring trions when the trion is considered as a charge-exciton system and the resultant repulsive trion-trion interaction.

$-\frac{ke}{\kappa}\frac{\mathbf{R}\cdot\mathbf{d}}{R^3}$ and $V_{\rm dd}(\mathbf{R}) \xrightarrow[R\to\infty]{} \frac{k}{\kappa}\frac{1}{R^3}[\mathbf{d}_1\cdot\mathbf{d}_2 - 3\frac{(\mathbf{R}\cdot\mathbf{d}_1)(\mathbf{R}\cdot\mathbf{d}_2)}{R^2}]$. Thus, the attractive interactions between a charge carrier from one trion with the dipole in the neighboring trion and the repulsive dipole-dipole interaction between two neighboring trions are proportional to $-1/R^2$ and $1/R^3$, respectively. Considering the trions as a charge-exciton system, in Fig. 7 we present 2D and 3D plots for the charge-charge, charge-dipole, and dipole-dipole interactions. In calculations we use the average value of the exciton dipole moment, and we assumed that exciton dipole moments in the neighboring trion are parallel. Even this simplified model shows that at $R > r_s$, the trion-trion interaction is repulsive and has a long-range Coulomb tail. In this approximation, one can replace the electrostatic repulsion between neighboring trions induced by their charge-carrier interactions by the electrostatic repulsion between the c.m. of two neighboring trions. Therefore, we can treat the dilute system of the charged spin-1/2 fermions interacting with the pair electrostatic repulsion formed by the trions in the same way as the dilute system of electrons.

As previously shown for the system of 2D electron gas [126], the qualitative criterion of the stability of the WC is the condition when the average potential energy exceeds the average kinetic energy: $\langle U \rangle > \langle K \rangle$, where $\langle U \rangle$ and $\langle K \rangle$ are the average value of the potential and kinetic energies, respectively. A dilute ensemble of repulsively interacting trions forms a Wigner lattice when the average trion-trion interaction energy exceeds the average kinetic energy of the c.m. of trions. This condition allows us to determine the density at which the ensemble of repulsively interacting trions undergoes a Wigner crystallization.

Let us show that at zero temperature, a trion WC exists at higher densities than an electron (or hole) WC. Neglecting the rotational energy contribution, it is straightforward to get a qualitative picture of the trion Wigner crystallization by performing an analysis similar to that reported for the 2D electron gas. Previous studies found crystallization of electrons to occur at $r_s = 37$ a.u. [96], $r_s = 34$ a.u. [109], and $r_s = 31$ a.u. [114]. The latter value for r_s was obtained in the framework of quantum Monte Carlo methods to calculate the zero-temperature phase diagram of the two-dimensional homogeneous electron gas. Estimating U and K for the trion system analogously to the electron system [96], we conclude that the 2D trion WC is stable when the dimensionless density parameter $r_s \geqslant 37$ at $T = 0$. The Wigner-Seitz radius is defined as $r_s = a/a_0$, where $a = (\pi\rho)^{-1/2}$ is the average distance between the c.m. of trions, ρ is the 2D density of trions, and $a_0 = 4\pi\varepsilon_0\hbar^2/[M(E_\perp)e^2]$ is the effective Bohr radius, where $M(E_\perp)$ is the mass of the trion that can be controlled by the external electric field. The last condition enables us to determine the density at which the trion gas becomes a WC. Moreover, by varying the external electric field, one can obtain a desirable density of a trion gas. For example, at $E_\perp = 2.5$ V/Å the mass of each charge carrier is about $0.5m$ and $0.8m$, where m is the mass of a free electron, in Si and Ge, respectively. For trions in silicene and germanene, this condition corresponds to $\rho \leqslant 1.9 \times 10^{13}$ cm^{-2} and $\rho \leqslant 4.8 \times 10^{13}$ cm^{-2}, respectively. For the electron Wigner crystal, we substitute $a_0 = 4\pi\hbar^2\varepsilon_0/m_A(E_\perp)(e^2)$, which results in $\rho \leqslant 2.1 \times 10^{12}$ cm^{-2} and $\rho \leqslant 5.4 \times 10^{12}$ cm^{-2} for Si and Ge, respectively. Therefore, the trion Wigner crystal can be

formed at sufficiently higher densities than an electron (or hole) WC, because the mass of a trion is greater than the effective mass of the electron or hole in the same Xene monolayer.

Above, we considered the trion gas at zero temperature and assumed that a 2D Wigner crystal in the ground state will have no defects. At finite temperatures, the defects will always destroy the long-range translational order in the 2D Wigner crystals. Let us mention that in practice it is challenging to experimentally realize a WC because quantum-mechanical fluctuations overpower the electrostatic repulsion and can quickly cause disorder.

IV. CONCLUSION

In summary, we predict the existence of electrically controlled trions in Xenes monolayers. We have applied the hyperspherical harmonics method to the calculation of BEs for the trion, and we predict the formation of trions in freestanding, supported, and encapsulated Xenes in an external electric field perpendicular to monolayers. The results of BE calculation for trions formed by A and B excitons show a non-negligible difference in trion energies that increases slightly as the electric field increases. The BEs of the intravalley and intervalley trions in the singlet state can be tuned in the range of 24–31 meV for silicene, 21–26 meV for germanene, and 14–20 meV for stanene by varying the external electric field from the critical value that is specific for each material up to 2.7 V/Å. Let us note that the trion binding energies in Xenes are the same order as in TMDC monolayers [38]. The dependence of the BE for silicene, germanene, and stanene as a function of the electric field is qualitatively similar. Our findings pave the way toward manipulating the trion BE by an external electric field.

The maximum BEs of intervalley triplet state trions are about 7.4 and 8.5 meV in silicene and germanene, respectively. In stanene, the triplet state trions are unbound. To understand the importance of the screened electron-hole interaction in the formation of trions in Xenes, we computed the BEs for Xenes supported on SiO_2 and encapsulated by hBN. It is demonstrated that the dielectric environment has a significant effect on the trion BE by decreasing it.

The results of calculations of the probability distribution show an increase in the compactness of trions with an increase of the electric field, since the greater binding energy increases the trion formation probability. We discussed and estimated the density of trion gas as composite fermions for the possibility of obtaining the Wigner crystallization of Xenes trions. The ensemble of repulsively interacting trions can form the Wigner lattice in an external electric field when their average interaction energy exceeds the average c.m. kinetic energy.

[1] M. A. Lampert, Mobile and immobile effective-mass-particle complexes in nonmetallic solids, Phys. Rev. Lett. **1**, 450 (1958).

[2] A. Kormányos, G. Burkard, M. Gmitra, J. Fabian, V. Zólyomi, N. D. Drummond, and V. Fal'ko, **k**·**p** theory for two-dimensional transition metal dichalcogenide semiconductors, 2D Mater. **2**, 022001 (2015).

[3] G. Wang, A. Chernikov, M. M. Glazov, T. F. Heinz, X. Marie, T. Amand, and B. Urbaszek, Excitons in atomically thin transition metal dichalcogenides, Rev. Mod. Phys. **90**, 021001 (2018).

[4] K. F. Mak, K. He, C. Lee *et al.*, Tightly bound trion in monolayer MoS_2, Nat. Mater. **12**, 207 (2013).

[5] H. Yu, X. Cui, X. Xu, and W. Yao, Valley excitons in two-dimensional semiconductors, Natl. Sci. Rev. **2**, 57 (2015).

[6] T. C. Berkelbach and D. R. Reichman, Optical and excitonic properties of atomically thin transition-metal dichalcogenides, Annu. Rev. Condens. Matter Phys. **9**, 379 (2018).

[7] M. V. Durnev and M. M. Glazov, Excitons and trions in two-dimensional semiconductors based on transition metal dichalcogenides, Phys. Usp. **61**, 825 (2018).

[8] R. Ya. Kezerashvili, Few-body systems in condensed matter physics, Few-Body Syst. **60**, 52 (2019).

[9] M. A. Semina and R. A. Suris, Localized excitons and trions in semiconductor nanosystems, Phys. Usp. **65**, 111 (2022).

[10] T. C. Berkelbach, M. S. Hybertsen, and D. R. Reichman, Theory of neutral and charged excitons in monolayer transition metal dichalcogenides, Phys. Rev. B **88**, 045318 (2013).

[11] A. Ramirez-Torres, V. Turkowski, and T. S. Rahman, Time-dependent density-matrix functional theory for trion excitations: application to monolayer MoS_2 and other transition-metal dichalcogenides, Phys. Rev. B **90**, 085419 (2014).

[12] M. Z. Mayers, T. C. Berkelbach, M. S. Hybertsen, and D. R. Reichman, Binding energies and spatial structures of small carrier complexes in monolayer transition-metal dichalcogenides via diffusion Monte Carlo, Phys. Rev. B **92**, 161404(R) (2015).

[13] I. Kylänpää and H.-P. Komsa, Binding energies of exciton complexes in transition metal dichalcogenide monolayers and effect of dielectric environment, Phys. Rev. B **92**, 205418 (2015).

[14] K. A. Velizhanin and A. Saxena, Excitonic effects in 2D semiconductors: Path integral Monte Carlo approach, Phys. Rev. B **92**, 195305 (2015).

[15] D. K. Zhang, D. W. Kidd, and K. Varga, Excited biexcitons in transition metal dichalcogenides, Nano Lett. **15**, 7002 (2015).

[16] B. Ganchev, N. Drummond, I. Aleiner, and V. Fal'ko, Three-particle complexes in two-dimensional semiconductors, Phys. Rev. Lett. **114**, 107401 (2015).

[17] D. W. Kidd, D. K. Zhang, and K. Varga, Binding energies and structures of two-dimensional excitonic complexes in transition metal dichalcogenides, Phys. Rev. B **93**, 125423 (2016).

[18] M. Szyniszewski, E. Mostaani, N. D. Drummond, and V. I. Fal'ko, Binding energies of trions and biexcitons in two-dimensional semiconductors from diffusion quantum Monte Carlo calculations, Phys. Rev. B **95**, 081301(R) (2017).

[19] E. Mostaani, M. Szyniszewski, C. H. Price, R. Maezono, M. Danovich, R. J. Hunt, N. D. Drummond, and V. I. Falko, Diffusion quantum Monte Carlo study of excitonic complexes

in two-dimensional transition-metal dichalcogenides, Phys. Rev. B **96**, 075431 (2017).

[20] T. Deilmann and K. S. Thygesen, Dark excitations in monolayer transition metal dichalcogenides, Phys. Rev. B **96**, 201113(R) (2017).

[21] R. Ya. Kezerashvili and S. M. Tsiklauri, Trion and biexciton in monolayer transition metal dichogenides, Few-Body Syst. **58**, 18 (2017).

[22] M. Donck, M. Zarenia, and F. Peeters, Excitons, trions, and biexcitons in transition-metal dichalcogenides: Magnetic-field dependence, Phys. Rev. B **97**, 195408 (2018).

[23] L. S. R. Cavalcante, D. R. da Costa, G. A. Farias, D. R. Reichman, and A. Chaves, Stark shift of excitons and trions in two-dimensional materials, Phys. Rev. B **98**, 245309 (2018).

[24] M. Florian, M. Hartmann, A. Steinhoff *et al.*, The dielectric impact of layer distances on exciton and trion binding energies in van der Waals heterostructures, Nano Lett. **18**, 2725 (2018).

[25] I. Filikhin, R. Ya. Kezerashvili, S. M. Tsiklauri, and B. Vlahovic, Trions in bulk and monolayer materials: Faddeev equations and hyperspherical harmonics, Nanotechnology **29**, 124002 (2018).

[26] A. Torche and G. Bester, First-principles many-body theory for charged and neutral excitations: Trion fine structure splitting in transition metal dichalcogenides, Phys. Rev. B **100**, 201403(R) (2019).

[27] D. Van Tuan, A. M. Jones, M. Yang, X. Xu, and H. Dery, Virtual trions in the photoluminescence of monolayer transition-metal dichalcogenides, Phys. Rev. Lett. **122**, 217401 (2019).

[28] J. Fu, J. M. R. Cruz, and F. Qu, Valley dynamics of different trion species in monolayer WSe$_2$, Appl. Phys. Lett. **115**, 082101 (2019).

[29] J. Yan and K. Varga, Excited-state trions in two-dimensional materials, Phys. Rev. B **101**, 235435 (2020).

[30] Y. V. Zhumagulov, A. Vagov, D. R. Gulevich, P. E. Faria Junior, and V. Perebeinos, Trion induced photoluminescence of a doped MoS$_2$ monolayer, J. Chem. Phys. **153**, 044132 (2020).

[31] Y. V. Zhumagulov, A. Vagov, N. Yu. Senkevich, D. R. Gulevich, and V. Perebeinos, Three-particle states and brightening of intervalley excitons in a doped MoS$_2$ monolayer, Phys. Rev. B **101**, 245433 (2020).

[32] M. Glazov, Optical properties of charged excitons in two-dimensional semiconductors, J. Chem. Phys. **153**, 034703 (2020).

[33] M. Van der Donck, M. Zarenia, and F. M. Peeters, Excitons and trions in monolayer transition metal dichalcogenides: A comparative study between the multiband model and the quadratic single-band model, Phys. Rev. B **96**, 035131 (2017).

[34] Y.-W. Chang and Y.-C. Chang, Variationally optimized orbital approach to trions in two-dimensional materials, J. Chem. Phys. **155**, 024110 (2021).

[35] F. Marsusi, E. Mostaani, and N. D. Drummond, Quantum Monte Carlo study of three-dimensional Coulomb complexes: Trions and biexcitons, hydrogen molecules and ions, helium hydride cations, and positronic and muonic complexes, Phys. Rev. A **106**, 062822 (2022).

[36] M. A. Semina, J. V. Mamedov, and M. M. Glazov, Excitons and trions with negative effective masses in two-dimensional semiconductors, Oxford Open Mater. Sci. **3**, itad004 (2023).

[37] K. Mohseni, M. R. Hadizadeh, T. Frederico, D. R. da Costa, and A. J. Chaves, Trion clustering structure and binding energy in two-dimensional semiconductor materials: Faddeev equations approach, Phys. Rev. B **107**, 165427 (2023).

[38] R. Ya. Kezerashvili, S. M. Tsiklauri, and A. Dublin, Trions in two-dimensional monolayers within the hyperspherical harmonics method: Application to transition metal dichalcogenides, Phys. Rev. B **109**, 085406 (2024).

[39] A. Molle, J. Goldberger, M. Houssa, Y. Xu, S.-C. Zhang, and D. Akinwande, Buckled two-dimensional Xene sheets, Nat. Mater. **16**, 163 (2017).

[40] J. Zheng, Y. Xiang, C. Li, R. Yuan, F. Chi, and Y. Guo, All-optically controlled topological transistor based on Xenes, Phys. Rev. Appl. **14**, 034027 (2020).

[41] L. Matthes, O. Pulci, and F. Bechstedt, Massive Dirac quasiparticles in the optical absorbance of graphene, silicene, germanene, and tinene, J. Phys.: Condens. Matter **25**, 395305 (2013).

[42] A. Acun, B. Poelsema, H. J. W. Zandvliet, and R. van Gastel, The instability of silicene on Ag(111), Appl. Phys. Lett. **103**, 263119 (2013).

[43] L. Tao, E. Cinquanta, D. Chiappe, C. Grazianetti, M. Fanciulli, M. Dubey, A. Molle, and D. Akinwande, Silicene field-effect transistors operating at room temperature, Nat. Nanotechnol. **10**, 227 (2015).

[44] B. Aufray, A. Kara, S. Vizzini, H. Oughaddou, C. Léandri, B. Ealet, and G. Le Lay, Graphene-like silicon nanoribbons on Ag(110): A possible formation of silicene, Appl. Phys. Lett. **96**, 183102 (2010).

[45] P. De Padova, C. Quaresima, C. Ottaviani, P. M. Sheverdyaeva, P. Moras, C. Carbone, D. Topwal, B. Olivieri, A. Kara, H. Oughaddou, B. Aufray, and G. Le Lay, Evidence of graphene-like electronic signature in silicene nanoribbons, Appl. Phys. Lett. **96**, 261905 (2010).

[46] N. D. Drummond, V. Zólyomi, and V. I. Fal'ko, Electrically tunable band gap in silicene, Phys. Rev. B **85**, 075423 (2012).

[47] M. Ezawa, Valley-polarized metals and quantum anomalous Hall effect in silicene, Phys. Rev. Lett. **109**, 055502 (2012).

[48] M. E. Dávila, L. Xian, S. Cahangirov, A. Rubio, and G. L. Lay, Germanene: A novel two-dimensional germanium allotrope akin to graphene and silicene, New J. Phys. **16**, 095002 (2014).

[49] A. J. Mannix, B. Kiraly, M. C. Hersam, and N. P. Guisinger, Synthesis and chemistry of elemental 2D materials, Nat. Rev. Chem. **1**, 0014 (2017).

[50] C. Grazianetti, C. Martella, and A. Molle, The Xenes generations: A taxonomy of epitaxial single-element 2D materials, Phys. Status Solidi RRL **14**, 1900439 (2020).

[51] D. Di Sante, X. Wu, M. Fink, W. Hanke, and R. Thomale, Triplet superconductivity in the Dirac semimetal germanene on a substrate, Phys. Rev. B **99**, 201106(R) (2019).

[52] L. Li, X. Wang, X. Zhao, and M. Zhao, Moiré superstructures of silicene on hexagonal boron nitride: A first-principles study, Phys. Lett. A **377**, 2628 (2013).

[53] A. I. Khan, T. Chakraborty, N. Acharjee, and S. Subrina, Stanene-hexagonal boron nitride heterobilayer: Structure and characterization of electronic property, Sci. Rep. **7**, 16347 (2017).

[54] S. Saxena, R. P. Chaudhary, and S. Shukla, Stanene: Atomically thick free-standing layer of 2D hexagonal tin, Sci. Rep. **6**, 31073 (2016).

[55] M. Ezawa, Quantum Hall effects in silicene, J. Phys. Soc. Jpn. **81**, 064705 (2012).

[56] R. Ya. Kezerashvili and A. Spiridonova, Effects of parallel electric and magnetic fields on Rydberg excitons in buckled two-dimensional materials, Phys. Rev. B **103**, 165410 (2021).

[57] F. Bechstedt, L. Matthes, P. Gori, and O. Pulci, Infrared absorbance of silicene and germanene, Appl. Phys. Lett. **100**, 261906 (2012).

[58] L. Stille, C. J. Tabert, and E. J. Nicol, Optical signatures of the tunable band gap and valley-spin coupling in silicene, Phys. Rev. B **86**, 195405 (2012).

[59] M. Fadaie, N. Shahtahmassebi, and M. R. Roknabad, Effect of external electric field on the electronic structure and optical properties of stanene, Opt. Quantum Electron. **48**, 440 (2016).

[60] D. Muoi, N. N. Hieu, C. V. Nguyen, B. D. Hoi, H. V. Nguyen, N. D. Hien, N. A. Poklonski, S. S. Kubakaddi, and H. V. Phuc, Magneto-optical absorption in silicene and germanene induced by electric and Zeeman fields, Phys. Rev. B **101**, 205408 (2020).

[61] S. Chowdhury and D. Jana, A theoretical review on electronic, magnetic and optical properties of silicene, Rep. Prog. Phys. **79**, 126501 (2016).

[62] X. Zhai, Y.-T. Wang, R. Wen, S.-X. Wang, Y. Tian, X. Zhou, W. Chen, and Z. Yang, Valley-locked thermospin effect in silicene and germanene with asymmetric magnetic field induced by ferromagnetic proximity effect, Phys. Rev. B **97**, 085410 (2018).

[63] A. Zhao and B. Wang, Two-dimensional graphene-like Xenes as potential topological materials, APL Mater. **8**, 030701 (2020).

[64] V. Y. Tsaran and S. G. Sharapov, Landau levels and magnetic oscillations in gapped Dirac materials with intrinsic Rashba interaction, Phys. Rev. B **90**, 205417 (2014).

[65] C.-H. Chen, W.-W. Li, Y.-M. Chang, C.-Y. Lin, S.-H. Yang, Y. Xu, and Y.-F. Lin, Negative-differential-resistance devices achieved by band-structure engineering in silicene under periodic potentials, Phys. Rev. Appl. **10**, 044047 (2018).

[66] J.-K. Lyu, S.-F. Zhang, C.-W. Zhang, and P.-J. Wang, Stanene: A promising material for new electronic and spintronic applications, Ann. Phys. (Berlin, Ger.) **531**, 1900017 (2019).

[67] N. R. Glavin, R. Rao, V. Varshney, E. Bianco, A. Apte, A. Roy, E. Ringe, and P. M. Ajayan, Emerging applications of elemental 2D materials, Adv. Mater. **32**, 1904302 (2020).

[68] C. Grazianetti, C. Martella, and A. Molle, Two-dimensional Xenes and their device concepts for future micro- and nanoelectronics and energy applications, in *Micro and Nano Technologies*, edited by L. Tao and D. Akinwande (Elsevier, Amsterdam, 2020), pp. 181–219.

[69] F. Bechstedt, P. Gori, and O. Pulci, Beyond graphene: Clean, hydrogenated and halogenated silicene, germanene, stanene, and plumbene, Prog. Surf. Sci. **96**, 100615 (2021).

[70] C.-C. Liu, W. Feng, and Y. Yao, Quantum spin Hall effect in silicene and two-dimensional germanium, Phys. Rev. Lett. **107**, 076802 (2011).

[71] M. Ezawa, Monolayer topological insulators: Silicene, germanene, and stanene, J. Phys. Soc. Jpn. **84**, 121003 (2015).

[72] L. Matthes, S. Küfner, J. Furthmüller, and F. Bechstedt, Quantization and topological states in the spin Hall conductivity of low-dimensional systems: An *ab initio* study, Phys. Rev. B **93**, 121106(R) (2016).

[73] F. Matusalem, D. S. Koda, F. Bechstedt, M. Marques, and L. K. Teles, Deposition of topological silicene, germanene and stanene on graphene-covered SiC substrates, Sci. Rep. **7**, 15700 (2017).

[74] X.-L. Yu, L. Huang, and J. Wu, From a normal insulator to a topological insulator in plumbene, Phys. Rev. B **95**, 125113 (2017).

[75] M. N. Brunetti, O. L. Berman, and R. Ya. Kezerashvili, Can freestanding Xene monolayers behave as excitonic insulators? Phys. Lett. A **383**, 482 (2019).

[76] M. N. Brunetti, O. L. Berman, and R. Ya. Kezerashvili, Optical properties of excitons in buckled two-dimensional materials in an external electric field, Phys. Rev. B **98**, 125406 (2018).

[77] O. Pulci, P. Gori, D. Grassano, M. D'Alessandro, and F. Bechstedt, Transitions in Xenes between excitonic, topological and trivial insulator phases: influence of screening, band dispersion and external electric field, SciPost Phys. **15**, 025 (2023).

[78] *Xenes:2D Synthetic Materials Beyond Graphene*, edited by A. Molle and C. Grazianetti, Woodhead Publishing Series in Electronic and Optical Materials (Elsevier Science, 2022).

[79] N. S. Rytova, Screened potential of a point charge in a thin film, Proc. MSU Phys., Astron. **3**, 30 (1967).

[80] L. V. Keldysh, Coulomb interaction in thin semiconductor and semimetal films, JETP Lett. **29**, 658 (1979).

[81] C. J. Tabert and E. J. Nicol, Dynamical polarization function, plasmons, and screening in silicene and other buckled honeycomb lattices, Phys. Rev. B **89**, 195410 (2014).

[82] A. H. Castro Neto, F. Guinea, N. M. R. Peres, K. S. Novoselov, and A. K. Geim, The electronic properties of graphene, Rev. Mod. Phys. **81**, 109 (2009).

[83] D. S. L. Abergel, V. Apalkov, J. Berashevich, K. Ziegler, and T. Chakraborty, Properties of graphene: a theoretical perspective, Adv. Phys. **59**, 261 (2010).

[84] M. Ezawa, A topological insulator and helical zero mode in silicene under an inhomogeneous electric field, New J. Phys. **14**, 033003 (2012).

[85] M. Ezawa, Spin-valley optical selection rule and strong circular dichroism in silicene, Phys. Rev. B **86**, 161407(R) (2012).

[86] M. Fogler, L. Butov, and K. Novoselov, High-temperature superfluidity with indirect excitons in van der Waals heterostructures, Nat. Commun. **5**, 4555 (2014).

[87] O. L. Berman and R. Ya. Kezerashvili, High-temperature superfluidity of the two component Bose gas in a transition metal dichalcogenide bilayer, Phys. Rev. B **93**, 245410 (2016).

[88] O. L. Berman and R. Ya. Kezerashvili, Superfluidity of dipolar excitons in a transition metal dichalcogenide double layer, Phys. Rev. B **96**, 094502 (2017).

[89] P. Cudazzo, I. V. Tokatly, and A. Rubio, Dielectric screening in two-dimensional insulators: implications for excitonic and impurity states in graphane, Phys. Rev. B **84**, 085406 (2011).

[90] J. Avery, *Hyperspherical Harmonics* (Kluwer Academic, Dordrecht, 1989).

[91] R. I. Jibuti and K. V. Shitikova, *Method of Hyperspherical Functions in Atomic and Nuclear Physics* (Energoatomizdat, Moscow, 1993) (in Russian).

[92] L. D. Faddeev and S. P. Merkuriev, *Quantum Scattering Theory for Several Particle Systems* (Kluwer Academic, Dordrecht, 1993).

[93] I. Filikhin, R. Ya. Kezerashvili, and B. Vlahovic, The charge and mass symmetry breaking in the $K K \bar{K}$ system, J. Phys. G **51**, 035102 (2024).

[94] S. Balendhran, S. Walia, H. Nili, S. Sriram, and M. Bhaskaran, Elemental analogues of graphene: silicene, germanene, stanene, and phosphorene, Small **11**, 640 (2015).

[95] Z. Ni, Q. Liu, K. Tang, J. Zheng, J. Zhou, R. Qin, Z. Gao, D. Yu, and J. Lu, Tunable bandgap in silicene and germanene, Nano Lett. **12**, 113 (2012).

[96] B. Tanatar and D. M. Ceperley, Ground state of the two-dimensional electron gas, Phys. Rev. B **39**, 5005 (1989).

[97] E. Wigner, On the interaction of electrons in metals, Phys. Rev. **46**, 1002 (1934).

[98] E. Y. Andrei, G. Deville, D. C. Glattli, F. I. B. Williams, E. Paris, and B. Etienne, Observation of a magnetically induced Wigner solid, Phys. Rev. Lett. **60**, 2765 (1988)

[99] V. Goldman, M. Santos, M. Shayegan, and J. Cunningham, Evidence for two-dimensional quantum Wigner crystal, Phys. Rev. Lett. **65**, 2189 (1990).

[100] F. I. B. Williams, P. A. Wright, R. G. Clark, E. Y. Andrei, G. Deville, D.C. Glattli, O. Probst, B. Etienne, C. Dorin, C. T. Foxon, and J. J. Harris, Conduction threshold and pinning frequency of magnetically induced Wigner solid, Phys. Rev. Lett. **66**, 3285 (1991).

[101] T. Smolénski, P. E. Dolgirev, C. Kuhlenkamp, A. Popert, Y. Shimazaki, P. Back *et al.*, Signatures of Wigner crystal of electrons in a monolayer semiconductor, Nature (London) **595**, 53 (2021).

[102] J. Sung, J. Wang, I. Esterlis, P. A. Volkov, G. Scuri, Y. Zhou *et al.*, Observation of an electronic microemulsion phase emerging from a quantum crystal-to-liquid transition, arXiv:2311.18069.

[103] Z. Xiang, H. Li, J. Xiao, M. H. Naik, Z. Ge, Z. He *et al.*, Quantum melting of a disordered Wigner solid, arXiv:2402.05456

[104] Y. Zhou, J. Sung, E. Brutschea, I. Esterlis, Y. Wang, G. Scuri *et al.*, Bilayer Wigner crystals in a transition metal dichalcogenide heterostructure, Nature (London) **595**, 48 (2021).

[105] X. Huang, T. Wang, S. Miao, C. Wang, Z. Li, Z. Lian *et al.*, Correlated insulating states at fractional fillings of the WS_2/WSe_2 moiré lattice, Nat. Phys. **17**, 715 (2021).

[106] S. Miao, T. Wang, X. Huang, D. Chen, Z. Lian, C. Wang, M. Blei *et al.*, Strong interaction between interlayer excitons and correlated electrons in WSe_2/WS_2 moiré superlattice, Nat. Commun. **12**, 1 (2021).

[107] I. Shapir, A. Hamo, S. Pecker, C. P. Moca, Ö. Legeza, G. Zarand, and S. Ilani, Imaging the electronic Wigner crystal in one dimension, Science **364**, 870 (2019).

[108] L. Swierkowski, D. Neilson, and J. Szymánski, Enhancement of Wigner crystallization in multiple-quantum-well structures, Phys. Rev. Lett. **67**, 240 (1991).

[109] F. Rapisarda and G. Senatore, Diffusion Monte Carlo study of electrons in two-dimensional layers, Aust. J. Phys. **49**, 161 (1996).

[110] G. Goldoni and F. M. Peeters, Wigner crystallization in quantum electron bilayers, Europhys. Lett. **37**, 293 (1997);**38**, 319 (1997).

[111] C. Attaccalite, S. Moroni, P. Gori-Giorgi, and G. B. Bachelet, Correlation energy and spin polarization in the 2D electron gas, Phys. Rev. Lett. **88**, 256601 (2002).

[112] Y. Noda and M. Imada, Quantum phase transitions to charge-ordered and Wigner-crystal states under the interplay of lattice commensurability and long-range Coulomb interactions, Phys. Rev. Lett. **89**, 176803 (2002).

[113] B. Valenzuela, S. Fratini, and D. Baeriswyl, Charge and spin order in one-dimensional electron systems with long-range Coulomb interactions, Phys. Rev. B **68**, 045112 (2003).

[114] N. D. Drummond and R. J. Needs, Phase diagram of the low-density two-dimensional homogeneous electron gas, Phys. Rev. Lett. **102**, 126402 (2009).

[115] M. Siegmund, M. Hofmann, and O. Pankratov, Density functional study of collective electron localization: Detection by persistent current, J. Phys.: Condens. Matter **21**, 155602 (2009).

[116] M. Zarenia, D. Neilson, B. Partoens, and F. M. Peeters, Wigner crystallization in transition metal dichalcogenides: a new approach to correlation energy, Phys. Rev. B **95**, 115438 (2017).

[117] J. Knörzer, M. J. A. Schuetz, G. Giedke, D. S. Wild, K. DeGreve, R. Schmidt, M. D. Lukin, and J. I. Cirac, Wigner crystals in two-dimensional transition-metal dichalcogenides: Spin physics and readout, Phys. Rev. B **101**, 125101 (2020).

[118] B. Padhi, R. Chitra, and P. W. Phillips, Generalized Wigner crystallization in moiré materials, Phys. Rev. B **103**, 125146 (2021).

[119] S. Brem and E. Malic, Terahertz fingerprint of monolayer Wigner crystals, Nano Lett. **22**, 1311 (2022).

[120] Y. Huang and S. Das Sarma, Electronic transport, metal-insulator transition, and Wigner crystallization in transition metal dichalcogenide monolayers, Phys. Rev. B **109**, 245431 (2024).

[121] O. L. Berman and R. Ya. Kezerashvili, Restricted three body problem in semiconductor heterostructure, Few-Body Syst. **50**, 407 (2011).

[122] O. L. Berman, R. Ya. Kezerashvili, and S. M. Tsiklauri, Trions in coupled quantum wells and Wigner crystallization, Int. J. Mod. Phys. B **28**, 1450064 (2014).

[123] I. V. Bondarev, O. L. Berman, R. Ya. Kezerashvili, and Yu. E. Lozovik, Crystal phases of charged interlayer excitons in van der Waals heterostructures, Commun. Phys. **4**, 134 (2021).

[124] I. V. Bondarev and Y. E. Lozovik, Magnetic-field-induced Wigner crystallization of charged interlayer excitons in van der Waals heterostructures, Commun. Phys. **5**, 315 (2022).

[125] R. Ya. Kezerashvili and V. Ya. Kezerashvili, Charge-dipole and dipole-dipole interactions in two-dimensional materials, Phys. Rev. B **105**, 205416 (2022).

[126] P. M. Platzman and H. Fukuyama, Phase diagram of the two-dimensional electron liquid, Phys. Rev. B **10**, 3150 (1974).